

Observation of Kondo condensation in a degenerately doped silicon metal

Received: 28 May 2021

Accepted: 16 December 2022

Published online: 06 February 2023

 Check for updates

Hyunsik Im^{1,2}✉, Dong Uk Lee³, Yongcheol Jo¹, Jongmin Kim¹,
Yonuk Chong⁴✉, Woon Song⁵, Hyungsang Kim¹, Eun Kyu Kim³✉,
Taewon Yuk³, Sang-Jin Sin³✉, Soonjae Moon³, Jonathan R. Prance⁶,
Yuri A. Pashkin⁶ & Jaw-Shen Tsai^{2,7}

When a magnetic moment is embedded in a metal, it captures nearby itinerant electrons to form a so-called Kondo cloud. When magnetic impurities are sufficiently dense that their individual clouds overlap with each other they are expected to form a correlated electronic ground state. This is known as Kondo condensation and can be considered a magnetic version of Bardeen–Cooper–Schrieffer pair formation. Here, we examine this phenomenon by performing electrical transport and high-precision tunnelling density-of-states spectroscopy measurements in a highly P-doped crystalline silicon metal in which disorder-induced localized magnetic moments exist. We detect the Kondo effect in the resistivity of the Si metal at temperatures below 2 K and an unusual pseudogap in the density of states with gap edge peaks below 100 mK. The pseudogap and peaks are tuned by applying an external magnetic field and transformed into a metallic Altshuler–Aronov gap associated with a paramagnetic disordered Fermi liquid phase. We interpret these observations as evidence of Kondo condensation followed by a transition to a disordered Fermi liquid.

The interplay of electron–electron interactions, disorder and spin correlation in solids is the origin of many competing ground states and phase transitions between them^{1–3}, which are typically observed in strongly correlated complex materials ranging from heavy-fermion compounds⁴ to high-temperature superconductors^{5,6}. An intriguing question in complex interacting systems is how the interactions of microscopic particles lead to macroscopic phenomena such as superconductivity, charge and spin density waves and heavy fermions. The Kondo effect very often plays a central role in understanding the correlated ground states of electron systems and electrical transport (Fig. 1). Doping is a versatile tool with which to address this question because of its ability to control the interaction strength and the way particles interact with each other and with external perturbations such as magnetic fields and pressure^{7,8}.

Here, we report observations of the Kondo interaction and an exotic Bardeen–Cooper–Schrieffer (BCS)-type pseudogap in highly P-doped degenerate silicon (Si:P) with doping concentrations of $n \approx 2\text{--}5 \times 10^{19} \text{ cm}^{-3}$ at very low temperatures (Methods). The existence and formation of magnetic moments in metallic Si:P are well understood in terms of Anderson's picture and well explained in the pioneering works of Bhatt and Lee and others^{9–12}. Because of the high doping concentration (higher than $\sim 2 \times 10^{19} \text{ cm}^{-3}$), the Fermi energy (E_F) in Si:P lies in the conduction band¹³, as it does in a metal (Supplementary Fig. 4a). In these circumstances, it is very likely that the local moments are entangled with the conduction electrons to form micrometre-sized Kondo clouds^{14,15} that overlap with each other (Fig. 1b), leading to a correlated ground state in the Si:P metal. In this work, tunnelling

¹Division of Physics and Semiconductor Science, Dongguk University, Seoul, Korea. ²The Institute of Physical and Chemical Research (RIKEN), Tsukuba, Japan. ³Department of Physics, Hanyang University, Seoul, Korea. ⁴SKKU Advanced Institute of Nanotechnology (SAINT), Sungkyunkwan University, Suwon, Korea. ⁵Korea Research Institute of Standards and Science, Daejeon, Korea. ⁶Department of Physics, Lancaster University, Lancaster, UK. ⁷Department of Physics, Tokyo University of Science, Tokyo, Japan. ✉e-mail: hyunsik7@dongguk.edu; yonuk@skku.edu; ek-kim@hanyang.ac.kr; sjsin@hanyang.ac.kr

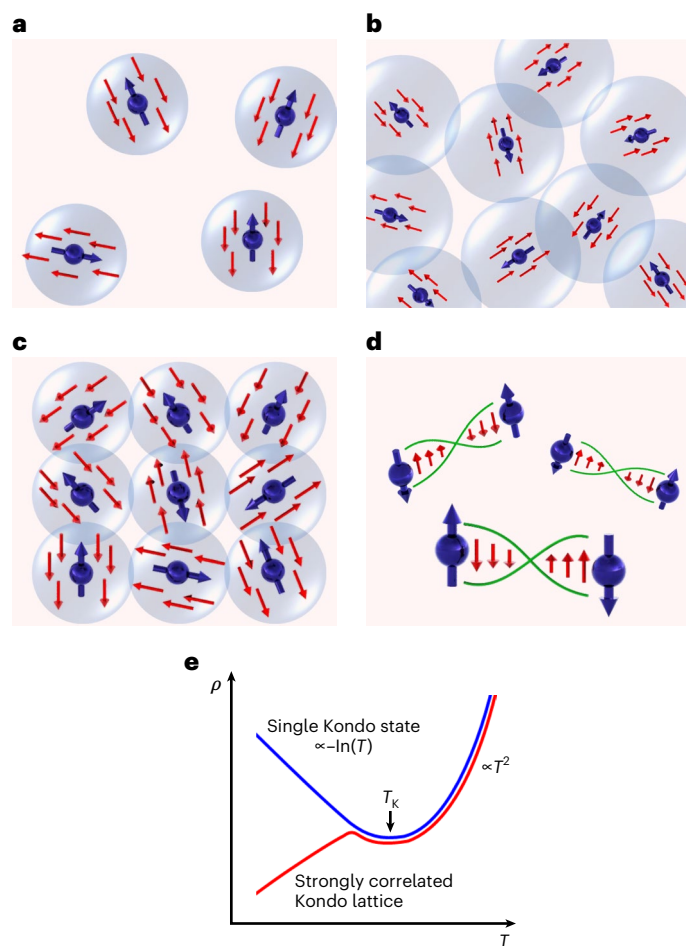


Fig. 1 | Schematics of different singlet states in metals with magnetic impurities. **a**, Non-overlapping Kondo singlet state. Kondo clouds are randomly distributed without interaction; this is practically the single-ion Kondo problem. Blue spheres and arrows indicate magnetic impurities; red arrows indicate conduction electrons. **b**, Overlapping Kondo singlet state (that is, Kondo condensation), where randomly distributed Kondo clouds overlap, interacting with each other and forming a correlated electron ground state. **c**, Kondo lattice. An electronic band of conduction electrons and a lattice of localized moments interact, forming a hybrid electronic structure. **d**, Random singlet state. Two adjacent impurities interact via the Ruderman–Kittel–Kasuya–Yosida (RKKY) interaction (green lines). The configuration of singlets in metals with magnetic moments is determined by many factors, such as the impurity density, randomness and complex interactions between electrons and impurities. **e**, Schematic illustration of the temperature-dependent resistivity $\rho(T)$ for two extreme cases: a non-overlapping Kondo singlet state and a correlated Kondo lattice. The single-impurity Kondo temperature T_K is identified experimentally as the resistivity minimum. For a Kondo lattice with a dense periodic array of magnetic moments (**c**), overlapping Kondo screening clouds lead to a heavy-fermion state and a downturn in the resistivity.

density-of-states (DOS) spectroscopy and bulk electrical transport measurements allow the electronic and magnetic nature of competing ground states in the Si:P metal to be explicitly identified and the relevant phase diagram in the temperature–magnetic field (T – B) plane to be constructed.

We first measured the differential resistance R_d of a bulk Si:P metal as a function of T and B . At $B = 0$ G, R_d exhibited strong temperature dependence at high temperatures (Fig. 2a). As T decreased below approximately 2 K, a clear anomaly appeared as a broadened step-like increase in R_d with decreasing T , and then it decreased slightly below ~1 K. As only a limited temperature range was available, the observed

step-like increase is difficult to describe analytically but the $\ln(T)$ behaviour (blue line) may be relevant. The temperature dependence of the resistance is reminiscent of that of a Kondo lattice compound with disorder¹⁶. The increase in $\ln(T)$ and the subsequent decrease in the resistivity of heavy-fermion compounds is attributed to Kondo scattering and the crossover to a coherent state of conduction and localized electrons. A modest magnetic field switches the non-Fermi liquid metal state to a conventional disordered Fermi liquid (DFL), confirming that the observed resistivity anomaly below 2 K is associated with magnetic interactions. On the other hand, the B -dependent R_d at 10 and 77 mK exhibited a small dip in the low-magnetic-field region (Fig. 2b), supporting the presence of the coupling of the local magnetic moments and conducting electrons. A similar magnetoresistance feature is observed in Ce-based heavy-fermion compounds and is attributed to magnetic quantum criticality¹⁷.

In fact, the interplay between the competing interactions may switch the ground state of the Si:P metal. The competition between the ground states can be elucidated by observing the evolution of tunnelling DOS spectra near E_F of the Si metal at various T and B . For this purpose, we fabricated tunnel junction devices consisting of the Si:P metal with silver (Ag) electrodes separated by a thin SiO_2 tunnel barrier for the tunnelling DOS spectroscopy measurements (Fig. 2c and Methods). We also conducted experiments with Al– SiO_2 –Si:P tunnel junctions that revealed the expected Al superconducting energy gap and proved that tunnelling was the major transport mechanism in such structures. Because Ag behaves similarly to a Fermi liquid with a flat DOS region in the vicinity of E_F , the measured differential tunnelling conductance G is directly proportional to the DOS of Si:P: $G(V) \propto \text{DOS}(E)$, where $E = E_F + eV$ (V is the voltage across the tunnel barrier and e is the elementary charge). Some of the basic results measured below 200 mK are presented in Fig. 2d,e, which displays the measured G – V characteristics at various temperatures at $B = 0$ G and an intensity plot of G in the T – V plane, respectively. At $T = 18$ mK, a partial depletion of the tunnelling DOS near E_F , which may be referred to as a pseudogap, is seen in the G – V characteristics near $V = 0$ V, and anomalous peaks appear outside the pseudogap. As T increases, the depleted DOS within the pseudogap is restored, and the peaks become closer in a nonlinear manner. Above ~160 mK, the U-shaped pseudogap with the side peaks changes into a $V^{1/2}$ -type Altshuler–Aronov gap (also called a zero-bias anomaly (ZBA))¹⁸, which is anticipated for metallic bulk Si with disorder and Coulomb correlations in the paramagnetic DFL phase.

Next, we present results that show how the anomalous DOS spectrum at E_F varies with B at $T = 18$ mK. Figure 3a,b presents examples of the measured G – V characteristics at various B below 3,000 G and an intensity plot of G in the B – V plane. As B increases, the peaks become closer together, and the depth and width of the U-shaped pseudogap decrease. Most noticeably, the pseudogap and peaks smoothly change into the Altshuler–Aronov ZBA of the paramagnetic DFL phase. Afterwards, the $|V|^{1/2}$ -dependent G – V curve remains unchanged and independent of B . Interestingly, in the intermediate B region between approximately 1,000 and 2,000 G, $G(V)$ increases linearly as a function of V up to the position of the considerably smaller peaks and then remains constant. Thus, this $|V|^{-1}$ -dependent G – V curve has a V-shaped groove, which is distinct from the ZBA. The inset in Fig. 3a shows a comparison of this V-shaped pseudogap and the ZBA. The depth and width of the V-shaped pseudogap continue to decrease with increasing B and T (Supplementary Fig. 5); however, its dependence on B is much weaker than that of the U-shaped pseudogap in the low- B region. We have confirmed that the observed anomalous DOS spectra are not hysteretic in B by sweeping B in both directions. Thus, the observed smooth B -driven phase transition, together with the electrical properties of a bulk Si:P metal, reveal that an exotic magnetically correlated state (which is not generally anticipated in a simple elemental semiconductor) seems to exist in the degenerately doped Si:P metal. T - and B -dependent characteristics

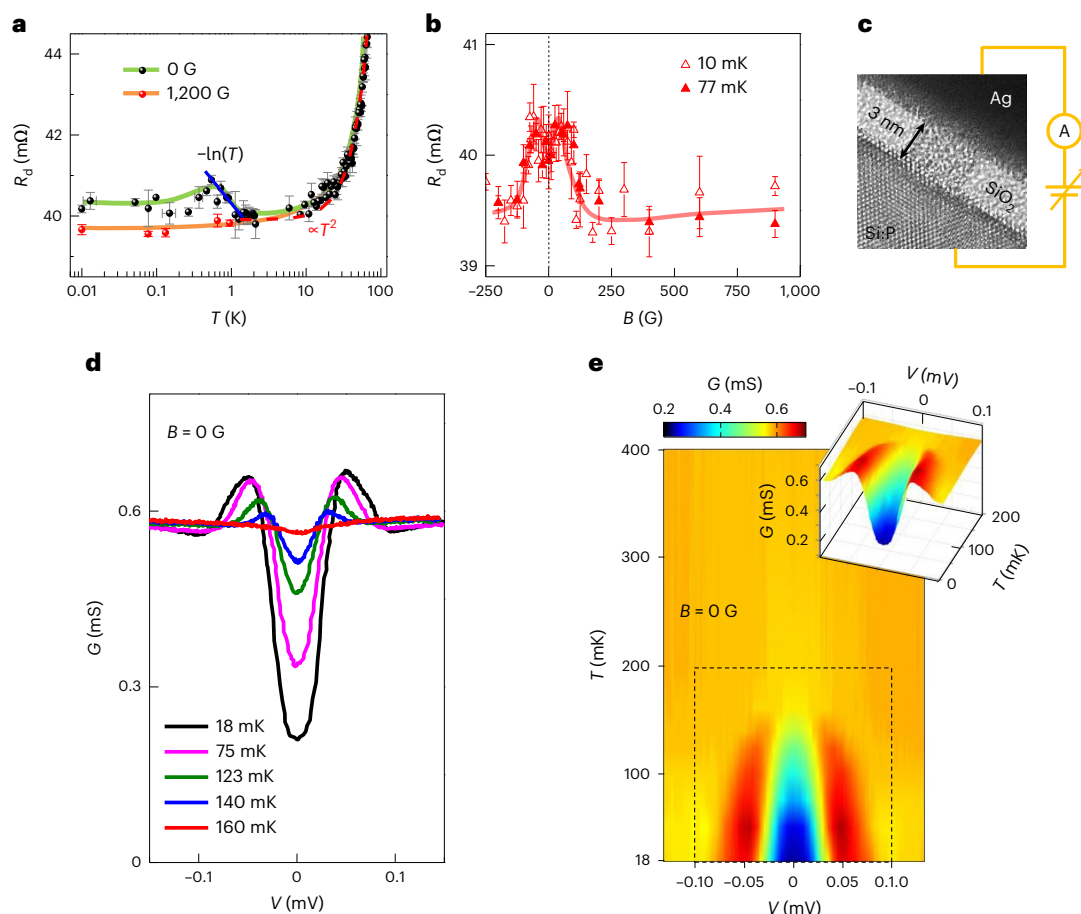


Fig. 2 | Single-particle DOS spectra and the bulk resistance of the Si:P metal.

a, Temperature-dependent R_d of bulk Si:P metal at $B = 0$ and 1,200 G, together with a fit according to the T^2 -dependent behaviour (red dotted line) and $\ln(T)$ (solid blue line). **b**, Magnetic-field-dependent R_d at 10 and 77 mK, showing a small dip in the low-magnetic-field regime. The solid lines are guides to the eye. Error bars in **a** and **b** represent the standard error of the mean due to repeated measurements (Supplementary Section 1). **c**, Cross-sectional high-resolution transmission electron microscopy image of a Ag–SiO₂–Si:P tunnel junction

device with a circuit diagram of single-particle DOS measurements. **d**, Tunneling conductance $G(V, B = 0 \text{ G})$ with decreasing temperature. Above $\sim 160 \text{ mK}$, a $|V|^{1/2}$ -type Altshuler–Aronov ZBA is observed in the DOS of Si:P near E_F . Upon cooling, a U-shaped pseudogap and DOS peaks are detected. **e**, Intensity map of the temperature-dependent $G(V, B = 0 \text{ G})$. The inset shows the three-dimensional enlarged view of the temperature-dependent $G(V, B = 0 \text{ G})$ curves in the low- T region.

of the pseudogap and anomalous peaks are presented in the Supplementary Figs. 6 and 7.

Nonlinear behaviour is observed in the B -dependent restoration of the DOS at E_F (G at $V = 0 \text{ V}$) at various T from 18 mK to 160 mK. The smooth magnetic phase transition from the magnetic pseudogap phase to the paramagnetic DFL phase is demonstrated in the intensity plot for the zero-bias differential conductance, $G(V, B)$, at 18 mK for each value of B (Supplementary Fig. 8). In the low- T region below approximately 100 mK, the DOS minimum (pseudogap) at E_F is reinstated superlinearly with B and then sublinearly up to the value of B (Supplementary Fig. 9a) at which the non-magnetic $|V|^{1/2}$ -dependent ZBA starts to appear in the DFL phase. There exists a clear inflection point (marked with the vertical arrows in the inset of Supplementary Fig. 9a) in the derivative of the $G(V = 0 \text{ V})-B$ curve, and we regard this point as the boundary between the superlinear (strongly B -dependent) and sublinear (weakly B -dependent) regions. As T increases, the inflection B point shifts to lower B values, making a boundary in the T - B plane (black diamonds in Supplementary Fig. 9b). The measured tunnelling conductance of Al–SiO₂–Si:P devices confirms a strong modification in the DOS near E_F of the Si:P metal (Supplementary Fig. 10).

The T - B phase diagram of the Si:P metal shown in Fig. 4 summarizes our main experimental results. Two different phases are clearly

visible in the intensity map of the DOS at E_F in the T - B plane with an intervening region. The blue region corresponds to the magnetic metal phase where the U-shaped pseudogap and large anomalous DOS peaks outside the gap appear. The black diamonds show the inflection point in the derivative of the $G(V = 0 \text{ V})-B$ curve as a function of T . In this phase, the DOS spectrum at E_F (G at $V = 0 \text{ V}$) changes strongly as B varies. The red stars represent the temperature at which the non-magnetic $|V|^{1/2}$ -type ZBA is detected first, T^* , at different B , creating the most important characteristic boundary between the magnetically correlated metal phase and the non-magnetic DFL phase. The magnetic metal phase transforms smoothly into the paramagnetic DFL phase (yellow region) through the intervening weakly magnetic metal phase (green region), where the V-shaped DOS spectrum appears with considerably weaker DOS peaks. In this intervening phase, the depleted DOS at E_F is reinstated relatively weakly with increasing B . The boundary consisting of the green circles indicates the temperature at which the anomalous DOS peaks are first detected (T_Δ ; Supplementary Fig. 6).

Observations of the abnormal electronic DOS spectra in the Si:P metal and their B -driven tuning are very surprising because neither the host Si nor the dopant P show a magnetic order in the crystal structure, and degenerate Si:P is regarded as a metal (E_F is located within the conduction band). We ruled out several possible mechanisms that

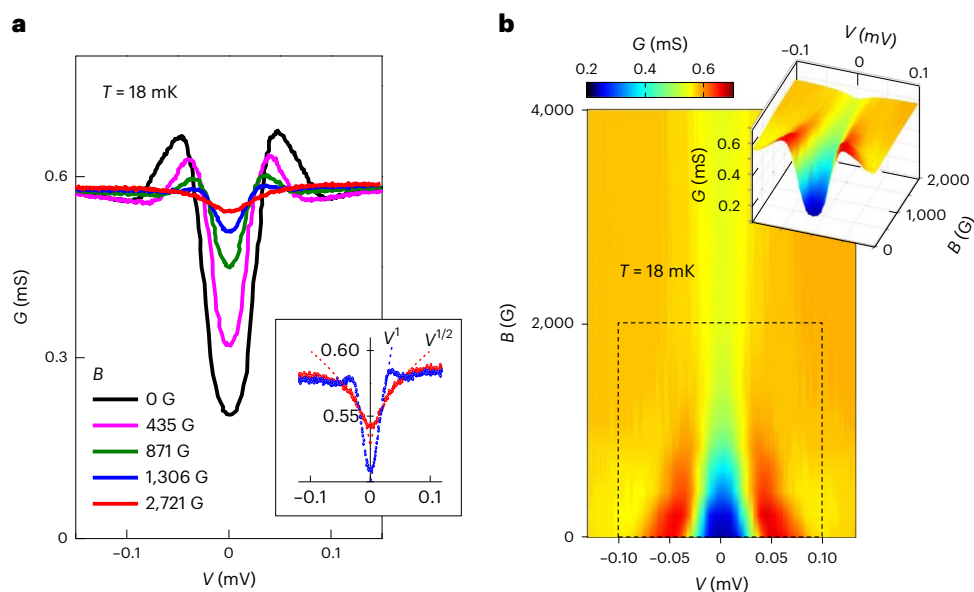


Fig. 3 | Magnetic field-driven phase transition. **a**, $G(V)$, $T = 18$ mK with increasing B . The inset shows an enlarged view of the $G(V)$ curves measured at $B = 1,306$ and $2,721$ G. The dotted lines are fitted to the curves using $|V|$ and $|V|^{1/2}$

relations. **b**, Intensity map of the B -dependent $G(V)$ at $T = 18$ mK. The inset shows the three-dimensional enlarged view of the B -dependent $G(V)$ curves in the low- B region.

could be responsible for our exotic DOS spectra. First, we ruled out a Coulomb gap scenario because it cannot explain the magnetic behaviour. Second, we ruled out spin glass-type magnetic gaps¹⁹ because no noticeable differences were seen between the field-cooled and zero-field-cooled DOS spectra. Neither of these mechanisms can explain the existence of DOS peaks outside the gap or the observed non-Fermi-liquid behaviours in the resistance of bulk Si:P. We also eliminated the possibility of the Kondo lattice gap because the local moments in our sample were randomly distributed. Indeed, our DOS was highly symmetric, while the DOS of the Kondo lattice system has a characteristic asymmetry²⁰. In fact, Si:P is not a heavy-fermion system. Third, the ground state with RKKY interaction-induced magnetic order, for example, the random singlet state (Fig. 1d), is not relevant because it does not have any gap at E_F (ref. 21). In addition, the spin density wave caused by the RKKY interaction may produce a BCS-like gap at E_F but the preliminary condition for such a mechanism is the lattice translation symmetry, which is absent in our Si metal due to random impurities. Finally, unlike boron (B)-doped degenerate Si (ref. 22), superconductivity has not been observed in P-doped Si and a clear signature of superconductivity (a collapse of the bulk resistance) was not also detected in our Si metal down to 10 mK. However, we do not entirely exclude the occurrence of incipient or hidden superconductivity.

All of the T - and B -dependent bulk transport, the DOS spectroscopy measurements and the existence of magnetic moments suggest that Kondo physics plays a key role in the formation of a correlated electron ground state in the Si:P metal. The underlying physics of the correlation behaviour is proposed here. That is, for a Si:P metal with a doping density of $\sim 3 \times 10^{19} \text{ cm}^{-3}$, more than a 10^{-5} fraction of the total impurities induce residual, unscreened localized moments⁹, and the mean distance between the moments is less than $1 \mu\text{m}$, which may be comparable to (or even smaller than) the size of a Kondo cloud. Our proposed ground state is the condensation of overlapping Kondo clouds (Fig. 1b), and as a consequence of Kondo condensation, a fraction of itinerant electrons entangled with magnetic impurities are correlated to form a many-body ground state. This Kondo condensation model is analogous to a Bose–Einstein condensate and, similar to BCS Cooper pairs, a singlet ground state with a small BCS-like gap is formed in the DOS at E_F . In fact, the shape and behaviour of the observed

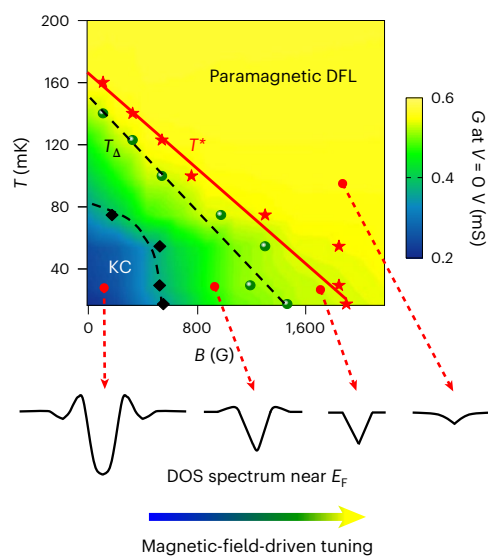


Fig. 4 | Magnetic phase diagram of the Si:P metal. Variation in the zero-bias conduction (namely, DOS at E_F in Si:P) in the T - B plane, showing the magnetic Kondo condensation (KC) phase (blue and green) and paramagnetic DFL phase. The magnetic transition line T^* (red stars) and the boundary (black diamonds) corresponding to the inflection points in the zero-bias $G(B)$ curves are plotted on the same phase diagram (see the text and Supplementary Fig. 9). The green circles represent T_K (Supplementary Fig. 6a). The applied magnetic field controls the magnetic correlations in the Si:P metal. Characteristic DOS spectra at E_F of Si:P in each phase region are shown below.

pseudogap in the Si:P metal is very similar to a BCS-like gap. In the lower doping regime where the metal–insulator transition occurs, this discovered ground state has not been reported. This is presumably because, although the density of magnetic impurities may be higher in this regime, the density of the itinerant electrons captured by the magnetic impurities to form Kondo clouds is not sufficiently high. This is the reason why the observed Kondo phenomenon occurs in the

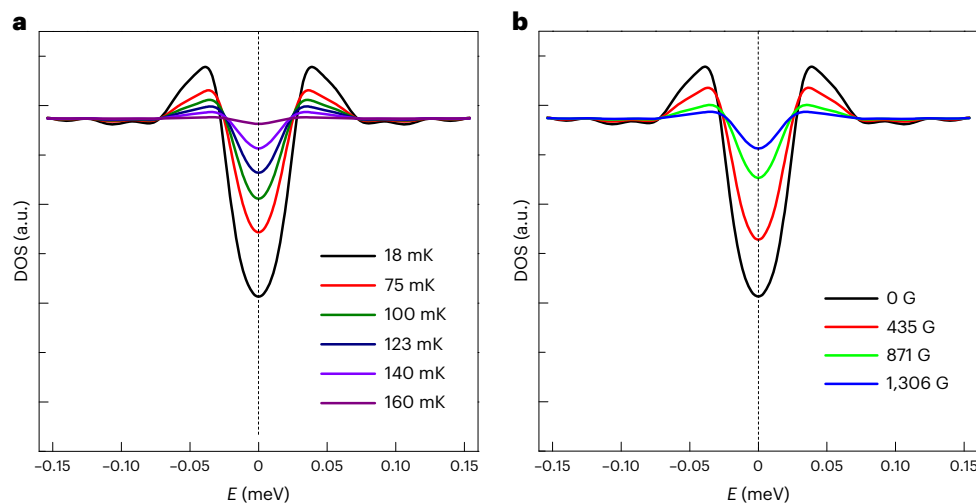


Fig. 5 | Theoretically calculated DOS spectra. **a**, Calculated DOS as a function of T at $B = 0$ G. **b**, Calculated DOS as a function of B at $T = 18$ mK. Here, $E = 0$ meV corresponds to E_F . For the data fitting at different temperatures, we modelled the temperature dependence of the condensation parameter, $M(T)$, as $M(T) = M_0(1 - T/T^*)^{1/2}$ where M_0 is a fitting parameter, which is universally true for any mean field theory including holographic theory. We chose M_0 such that the theory fitted the data at a particular temperature best, which we took as $T = 100$ mK. The same parameters were then used to see how the theory

could fit the data for other temperatures. Similarly, for the magnetic field evolution, we modelled the magnetic-field dependence of the condensation as $M(T) = M_0(1 - T/T^* - B/B_c)^{1/2}$, where T^* is the critical temperature at $B = 0$ G and similarly B_c is the critical field at $T = 0$ K. For calculations, we took $T^* = 147$ mK, $B_c = 1,600$ G and $M_0 = 5.44$. The magnetic phase boundary in the T - B plane (Fig. 4) is simply given by the $M = 0$ curve: $T/T^* + B/B_c = 1$. Note that the theory does not capture the transition to the ZBA in a DFL. a.u., arbitrary units.

degenerate metal regime, rather than the impurity band regime. To sum up, based on the tunnelling DOS and bulk transport measurements, as well as the fact that magnetic moments are present in the Si:P metal, the proposed microscopic picture responsible for the BCS-like DOS spectrum is Kondo condensation (that is, the overlap of randomly distributed Kondo clouds) and the mechanism for the zero-bias anomaly at elevated temperatures and magnetic fields is electron–electron interaction effects. Thus, the relevant balance between these competing ground states, which leads to a magnetic phase boundary, is controlled by the temperature and magnetic field—as demonstrated by the DOS in the T - B domain.

Understanding many-impurity Kondo physics at a microscopic level remains challenging, especially for disordered solids. In particular, the Kondo effect is a many-body interaction, so it would be inappropriate to apply a single-electron picture. The usual way to tackle the disorder effect is to consider the distribution of the Kondo temperature, which means that the system is described as a sum of independent subsystems with some probability of a given coupling. This is analogous to treating the system as a mixed state, which is an approximation that is only valid when the individual local components of the system (that is, individual Kondo clouds) do not correlate with each other. In such cases, the system can be treated as an ensemble of subsystems with random couplings, thus treating the disorder by summing over the random couplings⁹. However, the result of such approach is the scaling law in T , which seems to contradict our experimental finding: the observation of the BCS-like pseudogap that is convincing evidence for macroscopic coherence.

The Kondo condensation scenario proposed here can be used to reproduce the observed DOS spectra by considering the correlation effect on the spectrum of itinerant fermions. For this purpose, we introduce the charge neutral scalar field $\varphi = \langle c_{\uparrow} f_{\uparrow}^{\dagger} - c_{\downarrow} f_{\downarrow}^{\dagger} \rangle$, where c is an itinerant electron and f is an ion impurity with a net spin of $1/2$. Kondo condensation is the configuration in which φ is non-vanishing. If we consider φ as a constant part of field $\varphi(x)$, its coupling to the fermion can describe the effects of Kondo condensation on the spectrum of the fermion²³. When T or B increases sufficiently, the condensation is destroyed by thermal fluctuations or by Zeeman flips; thus, the

pseudogap will disappear, and the system will undergo a transition from a gapped scalar ordered state with Kondo condensation to a paramagnetic DFL state.

The calculation for the DOS spectra of this system encounters two sources of difficulty in many-body theories; that is, randomness and strong correlations. A mean-field description of the system that works even for a strongly interacting system would be helpful. One such theory is the holographic theory^{24–26}, the validity of which relies on the universality of the system near the quantum critical point. The principle of holography works even after the scale symmetry is slightly broken²⁷, similar to our situation where the scale symmetry is broken due to the presence of Kondo condensation (Supplementary Fig. 9). Figure 5a reveals the modelled pseudogap in the DOS and two DOS peaks at opposite energies, calculated at $B = 0$ V. A gap is clearly visible in the DOS at $T = 18$ mK, whereas for a larger value of $T > 160$ mK, the pseudogap is closed, which is in qualitative agreement with the experimental G - V curve at $B = 0$ G and $T = 18$ mK (Fig. 2d). Because there is a non-zero DOS value at E_F ($V = 0$ V), the corresponding state is a metal. For larger magnetic fields, no strong pseudogap is present in the computed DOS (Fig. 5b). The calculated magnetic-field-dependent DOS spectra are qualitatively similar to the experimental G - V curves (Fig. 3a). In addition to our holographic model, it will be worth checking the reproducibility of our results using other theoretical approaches (Supplementary Information 10).

In conclusion, similarly shaped DOS spectra at E_F have been observed in cuprate, pnictide and heavy-fermion superconductors^{5,6,28,29}. In fact, the T - B phase diagram of our Si:P metal in Fig. 4 is also similar to that of the quantum materials listed above. This result is not a surprise because the observed pseudogap behaviours in these materials can be commonly explained by coherent electronic states with a correlation. Although a microscopic understanding of how the order parameter depends on external perturbations such as T , B , pressure, and doping is still challenging, the observation of Kondo condensation and its phase transition in degenerately doped elemental semiconductor Si will contribute to understanding other quantum materials such as Kondo lattices, spin glasses and high- T_c superconductors. It would also be interesting to experimentally probe the Hall

coefficient and shot noise near the quantum critical point, which are expected to display non-Fermi liquid physics^{30–32}.

Online content

Any methods, additional references, Nature Portfolio reporting summaries, source data, extended data, supplementary information, acknowledgements, peer review information; details of author contributions and competing interests; and statements of data and code availability are available at <https://doi.org/10.1038/s41567-022-01930-3>.

References

- Kroha, J. in *The Physics of Correlated Insulators, Metals, and Superconductors* Modeling and Simulation Series Vol. 7 (eds Pavarini, E. et al.) 12.1–12.27 (Forschungszentrum Julich, 2017).
- Aoki, H. & Kamimura, H. *The Physics of Interacting Electrons in Disordered Systems* (Oxford Univ. Press, 1989).
- Coleman, P. *Introduction to Many-Body Physics* (Cambridge Univ. Press, 2015).
- Yang, Y.-f, Fisk, Z., Lee, H.-O., Thompson, J. D. & Pines, D. Scaling the Kondo lattice. *Nature* **454**, 611–613 (2008).
- Keimer, B., Kivelson, S. A., Norman, M. R., Uchida, S. & Zaanen, J. From quantum matter to high-temperature superconductivity in copper oxides. *Nature* **518**, 179–186 (2015).
- He, Y. et al. Fermi surface and pseudogap evolution in a cuprate superconductor. *Science* **344**, 608–611 (2014).
- Manyala, N., DiTusa, J., Appli, G. & Ramirez, A. Doping a semiconductor to create an unconventional metal. *Nature* **454**, 976–980 (2008).
- Löhneysen, H. V. Electron-electron interactions and the metal-insulator transition in heavily doped silicon. *Ann. Phys.* **523**, 599–611 (2011).
- Lakner, M., Löhneysen, H. V., Langenfeld, A. & Wölfle, P. Localized magnetic moments in Si:P near the metal-insulator transition. *Phys. Rev. B* **50**, 17064–17073 (1994).
- Anderson, P. W. Local moments and localized states. *Rev. Mod. Phys.* **50**, 191–201 (1978).
- Bhatt, R. N. & Lee, P. A. Scaling studies of highly disordered spin-½ antiferromagnetic systems. *Phys. Rev. Lett.* **48**, 344–347 (1982).
- Langenfeld, A. & Wölfle, P. Disorder-induced local magnetic moments in weakly correlated metallic systems. *Ann. Phys.* **4**, 43–52 (1995).
- Alexander, M. N. & Holcomb, D. F. Semiconductor-to-metal transition in *n*-type group IV semiconductors. *Rev. Mod. Phys.* **40**, 815–829 (1968).
- Affleck, I. in *Perspectives of Mesoscopic Physics* (eds Aharony, A. & Entin-Wohlman, O.) 1–44 (World Scientific, 2010).
- Borzenets, I. V. et al. Observation of the Kondo screening cloud. *Nature* **579**, 210–213 (2020).
- Nakatsuji, S. et al. Intersite coupling effects in a Kondo lattice. *Phys. Rev. Lett.* **89**, 106402 (2002).
- Sluchanko, N. E. et al. Anomalies of magnetoresistance in Ce-based heavy fermion compounds. *Low Temp. Phys.* **41**, 1011–1023 (2015).
- Altshuler, B. L. & Aronov, A. G. Zero bias anomaly in tunnel resistance and electron-electron interaction. *Solid State Commun.* **30**, 115–117 (1979).
- Oppermann, R. & Rosenow, B. Magnetic gaps related to spin glass order in fermionic systems. *Phys. Rev. Lett.* **80**, 4767–4770 (1998).
- Zhang, X. et al. Hybridization, inter-ion correlation, and surface states in the Kondo insulator SmB₆. *Phys. Rev. X* **3**, 011011 (2013).
- Uematsu, K. & Kawamura, H. Randomness-induced quantum spin liquid behavior in the *s*=1/2 random J₁-J₂ Heisenberg antiferromagnet on the square lattice. *Phys. Rev. B* **98**, 134427 (2018).
- Bustarret, E. et al. Superconductivity in doped cubic silicon. *Nature* **444**, 465–468 (2006).
- Fradkin, E. *Field Theories of Condensed Matter Physics* (Cambridge Univ. Press, 2013).
- Witten, E. Anti-de Sitter space and holography. *Adv. Theor. Math. Phys.* **2**, 253–291 (1998).
- Maldacena, J. M. The large N limit of superconformal field theories and supergravity. *Int. J. Theor. Phys.* **38**, 1113–1133 (1999).
- Zaanen, J., Liu, Y., Sun, Y. & Schalm, K. *Holographic Duality in Condensed Matter Physics* (Cambridge Univ. Press, 2015).
- Hartnoll, S. A., Herzog, C. P. & Horowitz, G. T. Building a holographic superconductor. *Phys. Rev. Lett.* **101**, 031601 (2008).
- Zhou, X. et al. Evolution from unconventional spin density wave to superconductivity and a pseudogaplike phase in NaFe_{1-x}Co_xAs. *Phys. Rev. Lett.* **109**, 037002 (2012).
- Zhou, B. B. et al. Visualizing nodal heavy fermion superconductivity in CeCoIn₅. *Nat. Phys.* **9**, 474–479 (2013).
- Paschen, S. et al. Hall-effect evolution across a heavy-fermion quantum critical point. *Nature* **432**, 881–885 (2004).
- Kirchner, S., Zhu, L., Si, Q. & Natelson, D. Quantum criticality in ferromagnetic single-electron transistors. *Proc. Natl Acad. Sci. USA* **102**, 18824–18829 (2005).
- Sela, E., Oreg, Y., von Oppen, F. & Koch, J. Fractional shot noise in the Kondo regime. *Phys. Rev. Lett.* **97**, 086601 (2006).

Publisher's note Springer Nature remains neutral with regard to jurisdictional claims in published maps and institutional affiliations.

Open Access This article is licensed under a Creative Commons Attribution 4.0 International License, which permits use, sharing, adaptation, distribution and reproduction in any medium or format, as long as you give appropriate credit to the original author(s) and the source, provide a link to the Creative Commons license, and indicate if changes were made. The images or other third party material in this article are included in the article's Creative Commons license, unless indicated otherwise in a credit line to the material. If material is not included in the article's Creative Commons license and your intended use is not permitted by statutory regulation or exceeds the permitted use, you will need to obtain permission directly from the copyright holder. To view a copy of this license, visit <http://creativecommons.org/licenses/by/4.0/>.

© The Author(s) 2023

Methods

Sample preparation and characterization

The structural, electrical and magnetic properties of bulk Si:P metal were studied using transmission electron microscopy, secondary ion mass spectrometry, magnetoresistance and superconducting quantum interference device measurements (Supplementary Figs. 1–3). Tunnel junction devices were fabricated on a [100]-oriented Si substrate with a P concentration of $\sim 2.6 \times 10^{19} \text{ cm}^{-3}$. The SiO₂ tunnel barrier was formed by thermal oxidation of the Si:P layer. The tunnel junction device was then completed by depositing a 200-nm-thick top Ag or Al electrode.

Data availability

The datasets generated and/or analysed during this study are available from the corresponding authors on reasonable request. Source data are provided with this paper.

Code availability

Codes for performing numeric calculations are available from the corresponding authors upon reasonable request.

Acknowledgements

We thank B. Altshuler, L. Ioffe, F. Nori, H. Aoki, H. Kamimura, V. Pudalov, M. Gershenson and H.-S. Sim for useful comments. This work was supported by the National Research Foundation of Korea (grant nos. 2021R1A4A5031805 (to H.I.), 2020R1A4A4078674 (to E.K.K.), 2021R1A2C1093652 (to E.K.K.), 2021R1A2B5B02002603 (to S.-J.S.), 2022H1D3A3A01077468 (to S.-J.S. and S.M.), 2022R1F1A1072865 (to S.M.), 2022M3E4A1083527 (to Y.C.) and 2022M3E4A1077186

(to Y.C.)). J.-S.T. was supported by a funding programme for the Japanese Cabinet Office ImPACT project.

Author contributions

H.I. planned the experiment, designed the samples and performed measurements and data analysis. D.U.L. fabricated the samples. Y.C., W.S., Y.J. and J.K. carried out measurements. H.K. contributed to the data analysis. E.K.K. directed the sample fabrication. Y.A.P., J.R.P. and J.-S.T. participated in experimental discussions and discussed the data. S.M. contributed to the physical interpretation. S.-J.S. provided a calculation scheme and wrote the theoretical sections. T.Y. performed calculations. H.I. directed the project and wrote the manuscript with contributions from all other co-authors.

Competing interests

The authors declare no competing interests.

Additional information

Supplementary information The online version contains supplementary material available at <https://doi.org/10.1038/s41567-022-01930-3>.

Correspondence and requests for materials should be addressed to Hyunsik Im, Yonuk Chong, Eun Kyu Kim or Sang-Jin Sin.

Peer review information *Nature Physics* thanks the anonymous reviewers for their contribution to the peer review of this work

Reprints and permissions information is available at www.nature.com/reprints.